Multi-Objective Robust Optimization of a Dual-Flux-Modulator Magnetic Geared Machine with Hybrid Uncertainties

Liu, Xiao; Zhao, Yunyun; Zhu, Jianguo; Chen, Zhe; Huang, Shoudao

Published in:
IEEE Transactions on Energy Conversion

DOI (link to publication from Publisher):
10.1109/TEC.2020.3003402

Publication date:
2020

Document Version
Accepted author manuscript, peer reviewed version

Multi-objective Robust Optimization of a Dual-Flux-Modulator Magnetic Geared Machine with Hybrid Uncertainties

Xiao Liu[1, *], Yunyun Zhao[1], Jianguo Zhu[2], Zhe Chen[3] and Shoudao Huang[1]
[1]Hunan University, College of Electrical and Information Engineering, Changsha, China
[2]University of Sydney, School of Electrical and Information Engineering, Sydney, Australia
[3]Aalborg University, Department of Energy Technology, Aalborg East, Denmark
xiaoliu@hnu.edu.cn*

***Abstract*—In order to improve the robustness and torque performance of a dual-flux-modulator magnetic-geared machine (DFM-MGM) considering simultaneously both random and interval uncertainties of design parameters, a multi-objective robust optimization (MORO) method with multiple Monte Carlo simulations (MCSs) is proposed. In this method, the multiple MCSs are adopted to evaluate the effects of parametric hybrid uncertainties on the robustness of optimization results. To build a MORO model of the DFM-MGM, the three-dimensional finite element model is established firstly and then validated by the experiment. Through a parametric study, it is found that five dimensional parameters of the permanent magnets (PMs) and stator have more significant effects on the stall torque (ST) and ST per PM volume (STPPV). Finally, a multi-objective particle swarm optimization algorithm with surrogate models, sigma criteria design and multiple MCSs method is implemented to solve the MORO problem. Both the average standard deviations and standard deviation differences of the ST and STPPV are used to deal with hybrid uncertainties during MORO. The optimized DFM-MGM by MORO has a STPPV 6.3% higher than that of the initial design under the same ST constraint. Moreover, the average standard deviations and standard deviation differences obtained by MORO are much smaller than those achieved by the deterministic optimization, indicating that the robustness of optimal results can also be significantly improved by the MORO.**

***Index Terms*--Dual-flux-modulator magnetic-geared machine, hybrid uncertainties, multi-objective robust optimization, robustness, torque performance.**

I. Introduction

In recent years, the magnetic-geared machines (MGMs), which integrate the coaxial magnetic gears (CMGs) in the permanent magnet (PM) electrical machines, are becoming promising power transmission devices for low-speed high-torque applications with the help of magnetic gearing effects [1]. The dual-flux-modulator MGM (DFM-MGM) presented in [2] shows higher static stall torque (ST) and higher rate of PM utilization than other types of MGMs. It was found that the torque capability of MGMs depended significantly on several dimensional parameters of the PMs and stator [3]. However, there is no such research on the DFM-MGM. Therefore, it is essential to conduct a parametric analysis and optimization for the DFM-MGM to improve the overall performance.

Several deterministic optimization designs for the CMGs and electric machines to maximize the performance have been conducted over the last decade [4-5]. The single objective deterministic design optimization method was applied to optimize a dual mechanical port machine with the aim to improve the torque performance [6]. The multi-objective deterministic optimization (MODO) has also been used to achieve the Pareto fronts for maximizing the power and minimizing the manufacturing cost of PM generators [7].

The deterministic optimization method mentioned above cannot consider clearly how the uncertainties of design variables affect the optimization process and results [8], whereas the torque capability [9] and mechanical deformation of electrical machines [10] are essentially affected by the uncertainties of design variables. Therefore, it is necessary to adopt the robust optimization design method involving the uncertainties of design parameters. Recently, a multi-objective robust optimization (MORO) method with six-sigma criteria was applied to improve the reliability and stability of PM machine design optimization [11] by treating the parameter uncertainties as random variables of normal distribution.

Although the conventional robust optimization has been applied in electrical machines to improve comprehensively the performance, the process may become less meaningful when the probability distributions cannot be formed due to the lack of sufficient data. Also, in an early stage of design, it can be difficult or impossible to acquire the probability distributions of the parameter uncertainties [12-13]. In this regard, the interval approach is often used because only the lower and upper bounds of the uncertainties of variables need to be set. A new robust optimization methodology namely the constrained formulation method was applied to find the robust optimal solution by considering only the interval variables [12]. An MORO was conducted to address the effects of interval uncertainty on the robust optimization results [13], by which the Pareto solutions could be achieved by considering the worst case.

Unfortunately, the parametric uncertainties are treated as either random variables or interval variables only in the above robust design optimization. In an actual application, however, both the random and interval uncertainties of design parameters can exist simultaneously [14]. The single objective robust design optimization involving hybrid uncertain variables for a mechanical structure was presented in [15]. Moreover, there exist also hybrid uncertainties caused by manufacturing and assembling of electrical machines, which need to be considered in robust optimal design of modern electrical machines. In addition, with an emphasis on the cost of electromagnetic

This article has been accepted for publication in a future issue of this journal, but has not been fully edited. Content may change prior to final publication. Citation information: DOI 10.1109/TEC.2020.3003402, IEEE Transactions on Energy Conversion

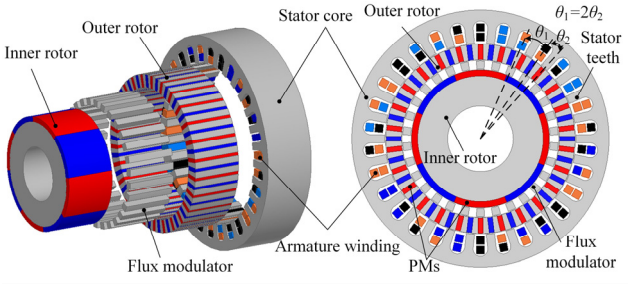

(a) (b)

Fig. 1. Topology of the DFM-MGM. (a) 3D exploded view and (b) cross-section view.

TABLE I
KEY PARAMETERS OF THE DFM-MGM

Quantity	Value (unit)
Pole-pair number of IR (p_{IR})	4
Pole-pair number of OR (p_{OR})	26
Pole-pair number of armature winding (p_a)	4
Pole-piece number of flux modulators (n_f)	30
Number of stator teeth (n_t)	30
Thickness of IR PMs (t_{IR})	6 mm
Pole-arc coefficient of IR (α_p)	1
Length of OR PMs (l_{OR})	15 mm
Width of OR PMs (w_{OR})	5 mm
Length of stator teeth (l_t)	21 mm
Length of stator yoke (l_y)	12 mm
Slot opening of flux modulators (θ_F)	6 °
Slot opening of stator teeth (θ_S)	5 °
Thickness of air-gaps	1 mm
Stack length	60 mm

devices, the ST and the utilization of PMs may conflict with each other [16-17]. Therefore, it is essential to improve the robustness of DFM-MGM design optimization by considering the random and interval uncertainties of design parameters, and simultaneously maximize the ST and ST per PM volume (STPPV).

Until now, no research on the MORO of electrical machines has been done with hybrid uncertainties. The MORO method is used to minimize the impact of hybrid uncertainties of design parameters on the torque performance of the DFM-MGM in this paper. The average means, average standard deviations and standard deviation differences of the torque performance are used to deal with hybrid uncertainties. In order to calculate both the average standard deviations and standard deviation differences of ST and STPPV, an MORO method combined with surrogate models, sigma criteria design and multiple Monte Carlo simulations (MCSs) is proposed to address the optimization problem considering the hybrid uncertainties of design parameters.

This paper is organized as follows. In Section II, a three-dimensional (3D) finite element (FE) model of the DFM-MGM is developed by using Maxwell, a commercial software of FE analysis, and validated by experimental results. Section III is devoted to the influence of design parameters of PMs and stator on the ST and STPPV. In Section IV, the multi-objective particle swarm optimization (MOPSO) algorithm is applied to optimize the DFM-MGM with the aim to improve simultaneously the robustness of design and torque performance considering the hybrid uncertainties. Finally, the

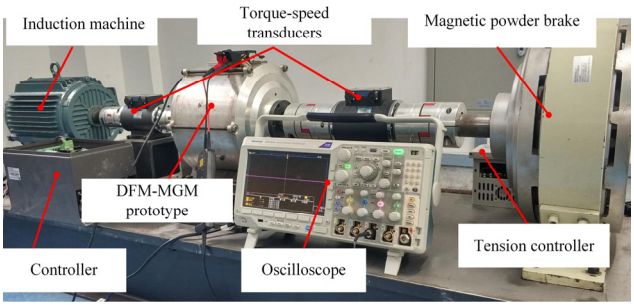

Fig. 2. Test rig for existing DFM-MGM.

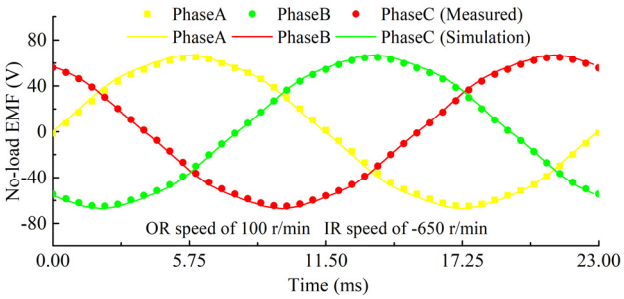

Fig. 3. Comparison with the simulation and measured no-load open-circuit EMF.

conclusion is drawn in Section V.

II. NUMERICAL MODELING OF THE DFM-MGM

A. FE modeling

The configuration of the studied DFM-MGM is shown in Fig. 1. The DFM-MGM has two rotors, one stationary flux modulator and one stator. Like the conventional CMGs, the stationary flux modulator is placed between the two rotors as the main flux modulator. The stator core functions as an auxiliary flux modulator which is fixed on the housing. The angle difference between the axis of stator teeth and pole-pieces on the main flux modulator (θ_2) is half of the pole-pieces pitch angle of the main flux modulator (θ_1), as shown in Fig. 1. The DFM-MGM employs surface-mounted PMs on the inner rotor (IR), that functions as an intermediate without any connection, but adopts spoke-type PMs on the outer rotor (OR) as the high torque output rotor. In order to eliminate the unbalanced magnetic pull, the studied DFM-MGM in this paper has 4 pole-pairs on the IR (p_{IR}) and 26 pole-pairs on the OR (p_{OR}), resulting in a theoretical gear ratio of 6.5. The number of uniformly pitched teeth on the stator surface is n_t. The number of pole-pairs of the IR (p_{IR}) is equal to the number of pole-pairs of the armature winding (p_a), and $n_t=p_a+p_{OR}$, such that the armature winding can be coupled with two rotors [2]. The rated current density of armature winding is set as 6 A/mm^2, and the initial design parameters of the DFM-MGM are given in Table I. Since the end-effects neglected by the two-dimensional FE method (FEM) may adversely affect the torque transmission capacity of the CMGs [18] and MGMs [19], in order to achieve high accuracy field analysis, the 3D FEM that takes into account the end-effects is used to calculate the ST and STPPV of the DFM-MGM. To verify the mesh independence of the FE

This article has been accepted for publication in a future issue of this journal, but has not been fully edited. Content may change prior to final publication. Citation information: DOI 10.1109/TEC.2020.3003402, IEEE Transactions on Energy Conversion

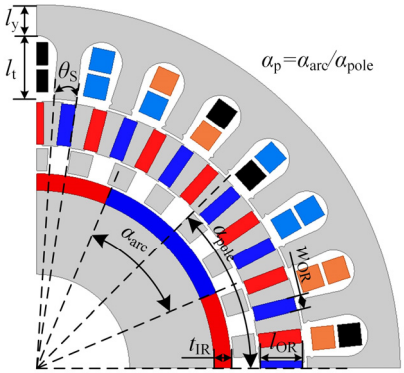

Fig. 4. Parametric analysis model of the DFM-MGM.

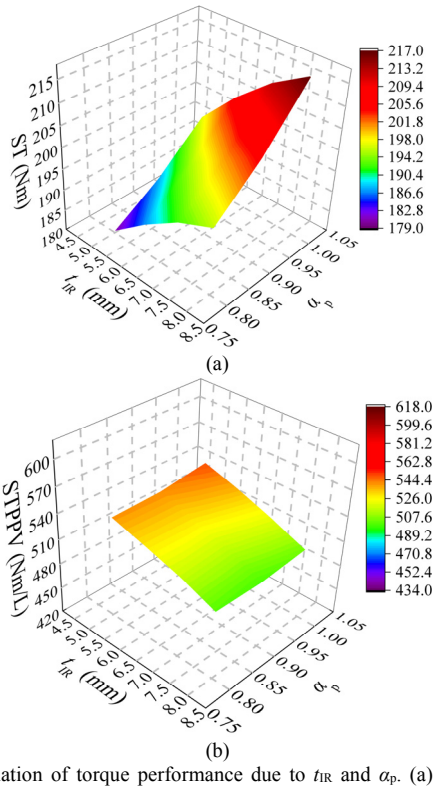

Fig. 5. Variation of torque performance due to t_{IR} and α_p. (a) ST and (b) STPPV.

model, the maximum lengths of global elements are set as 4.0, 3.0, 2.0 and 1.5 mm, respectively. Correspondingly, the total number of elements based on the above mesh setting are 909,032, 1,801,127, 4,081,412 and 6,282,645. When the current density is 6 A/mm^2, the ST on OR calculated by the 3D FEM are 190.8, 195.9, 205.5 and 205.6 Nm, respectively.

B. Validation of the FE model

Fig.2 shows a test rig for measuring the ST and no-load open-circuit back electromotive force (EMF) of the existing DFM-MGM. The measured ST on OR is 201.0 Nm at the rated current density. The errors between the measurement and FE analyses with the aforementioned maximum element lengths are 5.07%, 2.54%, 2.24% and 2.29%, respectively. When the maximum length of global elements is 2.0 mm, the relative error is only 2.24%, showing the acceptable mesh convergence and accuracy of 3D FE analysis. The corresponding simulated value of STPPV is 536.3 Nm/L. The experimental no-load

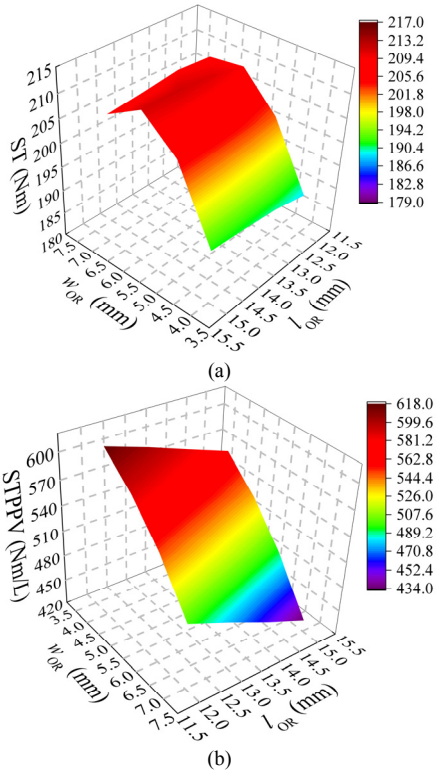

Fig. 6. Variation of torque performance due to w_{OR} and l_{OR}. (a) ST and (b) STPPV.

open-circuit EMF was measured when the IR was driven by an induction motor at the speed of 650 rev/min. As shown in Fig. 3, the three-phase EMFs predicted by the 3D FEM agree well with the experimental results with a relative error of 3.1%. The trade-off made on the manufacturing and assembling of the DFM-MGM accounts for these tiny discrepancies probably. The topological structure of DFM-MGM in the later sections of analysis and optimization is kept the same as that of the existing DFM-MGM, and only the geometric sizes vary. Therefore, the 3D FEM results are feasible for later sections.

III. Sensitivity Analysis

It has been proven that the torque capability of MGMs depends on several dimensional parameters significantly [6]. As shown in Fig. 4, the dimensional design parameters of t_{IR}, α_p, w_{OR}, l_{OR}, l_t, l_y and θ_T of the DFM-MGM are selected as the key design variables to be studied, while the other unstudied geometric parameters are kept the same as the initial design.

A. Effect of IR PMs dimensions

Fig. 5 presents the ST and STPPV of the DFM-MGM with different values of t_{IR} and α_p while the other parameters are fixed. Although the ST goes up with the increase of t_{IR} and α_p, α_p plays a much more important role than t_{IR} on ST, as shown in Fig. 5. Specifically, the STPPV decreases with the increase of t_{IR} due to the significant growth in the PM consumption. However, the STPPV can hardly be affected by α_p. In the case studied in this paper, the DFM-MGMs with (t_{IR}=8 mm, α_p=1.0) and (t_{IR}=5 mm, α_p=1.0) can achieve the highest ST and STPPV, respectively.

This article has been accepted for publication in a future issue of this journal, but has not been fully edited. Content may change prior to final publication. Citation information: DOI 10.1109/TEC.2020.3003402, IEEE Transactions on Energy Conversion

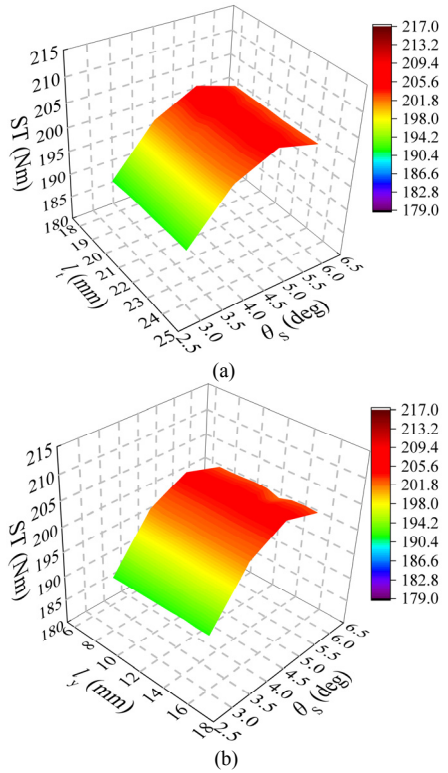

Fig. 7. Variation of the ST. (a) Due to l_t, θ_S and (b) due to l_y, θ_S.

B. Effect of OR PMs dimensions

The evolution of ST and STTPC of the DFM-MGM as a function of w_{OR} and l_{OR} varying within 4-7 mm and 12-15 mm, respectively, are shown in Fig. 6. As shown, the ST increases first and then decreases with the growth of w_{OR}, and the influence of l_{OR} on ST is similar to that shown in Fig. 5 (a). However, the STPPV decreases with the increase of w_{OR} and l_{OR} due to the significant growth of the PM volume, as shown in Fig. 6 (b). For the studied DFM-MGM, the design with w_{OR}=6 mm and l_{OR}=14 mm can achieve the highest ST, while the design with w_{OR}=4 mm and l_{OR}=12 mm achieves the highest STPPV.

C. Effect of stator dimensions

The 3D change trend curves of ST with varying l_t, θ_S and l_y, θ_S are shown in Figs. 7 (a) and (b), respectively, while keeping other parameters same as the initial design. As shown, the ST increases significantly first and then decreases with the increasing θ_S, but the ST hardly changes when l_t and l_y vary. As the parameters of θ_S, l_t and l_y exhibit no correlation with the PM volume, the variation trend of STPPV with these parameters will be the same as that shown in Fig. 7. The highest ST and STPPV can be achieved at θ_S=5° among the studied cases.

Through the above parametric analysis and discussion, the results clearly reveal that l_t and l_y have nearly no effect on the ST and STPPV of the studied DFM-MGM. However, it is found that ST and STPPV can be significantly affected by the following five parameters: t_{IR}, α_p, w_{OR}, l_{OR} and θ_S, which will be selected as the variables for further optimization.

IV. MORO OF THE DFM-MGM WITH HYBRID UNCERTAINTIES

Although the impacts of PM and stator parameters on ST and STPPV have been explored, it has not clearly found the robust optimal designs yet. Conventionally, the MODO with the Pareto fronts is employed to maximize the ST and STPPV. However, the MODO cannot consider the perturbations of design parameters and the robustness of optimization results to uncertainties. In the process of practical manufacturing and assembling, the hybrid uncertainties would exist. To increase the robustness and torque performance of DFM-MGM simultaneously, the MORO method must be used to deal with the hybrid uncertainties of variables.

A. Mechanism synthesis of MORO

The uncertain variables are typically classified as random and interval variables based upon the availability of the probabilistic characteristics [14]. Although it is difficult to acquire precisely the probability distributions of α_p due to the lack of knowledge about the center angle of arcuate IR PMs, the lower and upper limits of α_p could be obtained. Therefore, α_p is treated specially as an interval variable in this paper. Whilst other design parameters of t_{IR}, w_{OR}, l_{OR} and θ_S are considered as the random variables from the manufacturing perspectives. Typically, when the robustness of objectives, constraints and design variables are considered, while the other unselected parameters, i.e. the outer diameter of the stator and the lengths of internal and external air gaps, etc., are kept the same as the initial design, the MORO of DFM-MGM involving hybrid uncertainties of the design parameters can be formulated as the following:

$$\begin{cases} \min & -(1-\lambda_1-\lambda_2)\bar{\mu}[\frac{\mathrm{ST}}{\mathrm{ST}_{\mathrm{ref}}}]+\lambda_1\bar{\sigma}[\frac{\mathrm{ST}}{\mathrm{ST}_{\mathrm{ref}}}]+\lambda_2\delta(\sigma[\frac{\mathrm{ST}}{\mathrm{ST}_{\mathrm{ref}}}]), \\ & -(1-\lambda_1-\lambda_2)\bar{\mu}[\frac{\mathrm{STPPV}}{\mathrm{STPPV}_{\mathrm{ref}}}]+\lambda_1\bar{\sigma}[\frac{\mathrm{STPPV}}{\mathrm{STPPV}_{\mathrm{ref}}}]+\lambda_2\delta(\sigma[\frac{\mathrm{STPPV}}{\mathrm{STPPV}_{\mathrm{ref}}}]) \\ s.t. & 0.8 \le [\bar{\alpha}_p] \le 1.0 \\ & 5\ \mathrm{mm}+n\sigma[t_{IR}] \le \mu[t_{IR}] \le 8\ \mathrm{mm}-n\sigma[t_{IR}] \\ & 4\ \mathrm{mm}+n\sigma[w_{OR}] \le \mu[w_{OR}] \le 7\ \mathrm{mm}-n\sigma[w_{OR}] \\ & 12\ \mathrm{mm}+n\sigma[l_{OR}] \le \mu[l_{OR}] \le 15\ \mathrm{mm}-n\sigma[l_{OR}] \\ & 3\ \mathrm{deg}+n\sigma[\theta_S] \le \mu[\theta_S] \le 6\ \mathrm{deg}-n\sigma[\theta_S] \end{cases} \quad (1)$$

where μ is the mean, and λ_1 and λ_2 are the weighting coefficients imposed on the average standard deviation, $\bar{\sigma}$, and the difference between the maximum and minimum standard deviations, $\delta(\sigma)$, respectively. Since for low-speed high-torque applications of DFM-MGM, the high torque performance is more important, the weighting coefficients of the average means $\bar{\mu}$ for ST and STPPV are both set as 0.5, i.e. $\lambda_1+\lambda_2=0.5$. The reference values of ST and STPPV of the initial design, $\mathrm{ST}_{\mathrm{ref}}$ and $\mathrm{STPPV}_{\mathrm{ref}}$, are introduced to make two objectives comparable. Parameters $\bar{\mu}$, $\bar{\sigma}$ and $\delta(\sigma)$ can be defined by

$$\begin{cases} \bar{\mu} = \frac{1}{2}(\mu^{\max}+\mu^{\min}) \\ \bar{\sigma} = \frac{1}{2}(\sigma^{\max}+\sigma^{\min}) \\ \delta(\sigma) = \sigma^{\max}-\sigma^{\min} \end{cases} \quad (2)$$

This article has been accepted for publication in a future issue of this journal, but has not been fully edited. Content may change prior to final publication. Citation information: DOI 10.1109/TEC.2020.3003402, IEEE Transactions on Energy Conversion

TABLE II
ACCURACY ASSESSMENT OF THE SURROGATE MODELS

		RMSE	ME	R^2
KRG	ST	0.0326	0.0646	0.9691
	STPPV	0.0243	0.0489	0.9875
PR	ST	0.0177	0.0341	0.9968
	STPPV	0.0153	0.0316	0.9975
RBF	ST	0.0252	0.0419	0.9887
	STPPV	0.0199	0.0328	0.9946

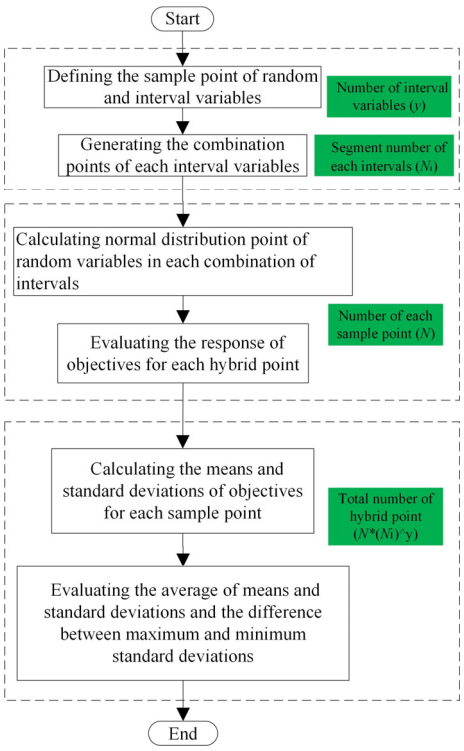

Fig. 8. Flow chart of the multiple MCSs procedure.

where μ^{max} and μ^{min} denote the maximum and minimum means, and σ^{max} and σ^{min} the maximum and minimum standard deviations, respectively. In order to enhance the robustness of optimization results effectively, the value of n is set as 6, namely 6σ, to control the width of distribution. The probability distribution of these random variables with the standard deviations as 1/6 of their manufacturing tolerances is given by the normal distribution. The tolerance values are equal to 5% of their variation ranges. For industrial manufacturing and assembling, the 6σ criteria signifies 0.002 defects per million for the short-term, and 3.4 defects per million for the long-term [20]. In this paper, the upper and lower variation ranges of the interval variable α_p equal 5% and -5% of $\bar{\alpha}_p$, respectively, where $\bar{\alpha}_p$ is the average of α_p. In the variation range of α_p, the distributions are assumed to be uniform and independent.

B. MORO methodology

Due to the high dimensionality and complexity of the DFM-MGM with two rotors, one flux modulator and one stator, it is difficult to optimize the DFM-MGM by the conventional analytical optimization method. The mathematical procedures assisted with surrogate modeling are widely used in the electric machines design [17]. The selection of sampling points is very important for establishing the surrogate models. Since the design of experiments (DOE) is an effective method for selecting the appropriate number of sample points, the full factorial design method as a DOE is adopted to generate 768 sample points for its uniformity in this study. Then, the ST and STPPV responses to these sampling points are obtained by the 3D FEM. Three different typical surrogate models, the Kriging (KRG), polynomial regression (PR) and radial basis function (RBF), are all constructed to approximate the responses of ST and STPPV, and the one with the highest accuracy is to be used for the subsequent optimization.

In this paper, to assess the accuracies of these surrogate models, the normalized root mean square error (RMSE), normalized maximum error (ME), and the square value (R^2) are adopted, which are defined by

$$\mathrm{RMSE}=\frac{\sqrt{\sum_{k=1}^{n}\left(y_k-\hat{y}_k\right)^2}}{n}\Big/\left(y_{k\_\max}-y_{k\_\min}\right) \tag{3}$$

$$\mathrm{ME}=\left(\frac{\max\left|y_k-\hat{y}_k\right|}{y_{k\_\max}-y_{k\_\min}}\right),\ k=1,2,\ldots,n \tag{4}$$

and

$$R^2=1-\frac{\sum_{k=1}^{n}\left(y_k-\hat{y}_k\right)^2}{\sum_{k=1}^{n}\left(y_k-\bar{y}_k\right)^2} \tag{5}$$

where y_k and $\hat{y}_k$ denote the results of FE analyses and surrogate models for new error analysis point k, respectively, $\bar{y}_k$ represents the average value of y_k, and n is the number of newly created assessment points. It can be noted that smaller normalized RMSE and ME are better, and the value of R^2 closer to 1 is more accurate for the surrogate models. In this paper, the additional error analysis points (n=30) are evenly generated by the optimal Latin hypercube design method for evaluating these surrogate models. The results of accuracy assessment for three surrogate models are listed in Table II. As shown, the PR surrogate models are the most accurate models, and the R^2 for the PR surrogate models of the ST and STPPV are 0.9968 and 0.9975, both very close to 1. Therefore, the PR surrogate models are reasonably accurate to predict these responses of ST and STPPV and will be employed in the subsequent MORO design for the DFM-MGM. The approximate functions of the ST and STPPV based on the PR surrogate models are expressed as

$$\begin{aligned}f_1(\theta_S,l_{OR},t_{IR},w_{OR},a_p)=&-78.43+20.91\theta_S+11.79l_{OR}+8.61t_{IR}+48.54w_{OR}-234.71a_p\\&-2.22\theta_S^2-0.24l_{OR}^2-0.77t_{IR}^2-4.05w_{OR}^2+139.63a_p^2+0.24\theta_Sl_{OR}+0.30\theta_St_{IR}+0.10\theta_Sw_{OR}\\&-2.15\theta_Sa_p-0.17l_{OR}t_{IR}-0.63l_{OR}w_{out}-1.29l_{OR}a_p+0.07t_{IR}w_{OR}+8.99t_{IR}a_p+9.98w_{OR}a_p\end{aligned} \tag{6}$$

$$\begin{aligned}f_2(\theta_S,l_{OR},t_{IR},w_{OR},a_p)=&1244.15+79.70\theta_S-24.71l_{OR}-39.81t_{IR}-4.76w_{OR}\\&-791.38a_p-6.02\theta_S^2+0.09l_{OR}^2-1.01t_{IR}^2-5.99w_{OR}^2+346.96a_p^2+0.17\theta_Sl_{OR}\\&+0.08\theta_St_{IR}-1.07\theta_Sw_{OR}-11.00\theta_Sa_p+1.55l_{OR}t_{IR}-2.14l_{OR}w_{out}+5.79l_{OR}a_p\\&+4.10t_{IR}w_{OR}-5.38t_{IR}a_p+39.66w_{OR}a_p\end{aligned} \tag{7}$$

where f_1 and f_2 are the approximate functions of ST and STPPV with the five design parameters, respectively.

The key to evaluate the robustness of optimization results is to translate the uncertainties of design variables into the

This article has been accepted for publication in a future issue of this journal, but has not been fully edited. Content may change prior to final publication. Citation information: DOI 10.1109/TEC.2020.3003402, IEEE Transactions on Energy Conversion

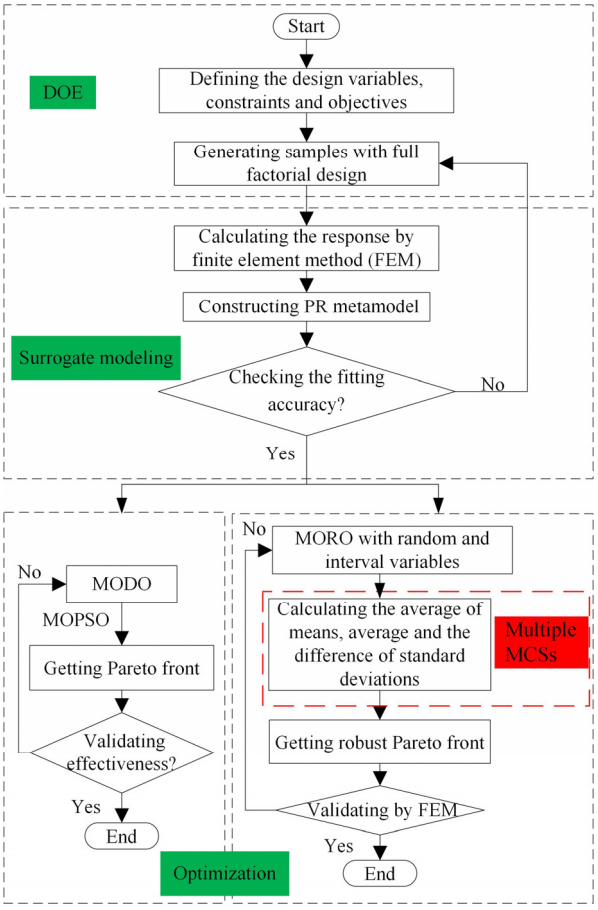

Fig. 9. Flow chart of the MODO and MORO with hybrid uncertainties.

TABLE III
MAIN SETTINGS OF MOPSO

Setting parameter	Value
Population size	100
External archive size	50
Inertial weight	0.730
Personal learning coefficient	1.496
Global learning coefficient	1.496

TABLE IV
OPTIMIZATION RESULT OF THE DESIGN PARAMETERS

Design parameter	MODO	MORO with $\lambda_1 = 0.45$ $\lambda_2 = 0.05$	MORO with $\lambda_1 = 0.05$ $\lambda_2 = 0.45$
t_{IR}	6.40 mm	6.92 mm	7.22 mm
α_p	1	1	0.98
w_{OR}	4.96 mm	4.68 mm	4.62 mm
l_{OR}	12.00 mm	12.15 mm	12.29 mm
θ_S	5.34°	5.67°	5.80°

uncertainties of predicted performance in the statistical characteristics. Among many existing methods, the Monte Carlo simulations (MCSs) are widely used as an effective method [8]. In order to assess the robustness of predicted response with the random and interval variables, a multiple MCSs method is proposed in this paper. Fig. 8 shows the flowchart of the multiple MCSs procedure for the robustness assessment, where each of the random and interval variables is assumed to be independent statistically. In this method, each interval variable is firstly divided into many small segments (N_i) to handle the interval variables. There are a total number of combinations of $(N_i)^y$ for all interval variables. Then, for each combination, these N are employed by the MCSs for all random variables, in which each random parameter is assumed to be distributed normally. Therefore, the numbers of hybrid points are equal to $N \times (N_i)^y$. For each combination of all interval variables, the means (μ) and standard deviations (σ) for the responses of ST and STPPV can be estimated by

$$\mu \cong \frac{1}{N}\sum_{j=1}^{N} f_Z \tag{8}$$

$$\sigma \cong \sqrt{\frac{1}{N-1}} \times \sqrt{\sum_{j=1}^{N}\left(f_Z - \mu\right)^2} \tag{9}$$

where f_z represents the responses of ST and STPPV. For each sample point, the number of μ and σ is equal to $(N_i)^y$. Finally, $\bar{\mu}$, $\bar{\sigma}$ and $\delta(\sigma)$ of the ST and STPPV can be obtained by (2). According to the values of $\bar{\mu}$, $\bar{\sigma}$ and $\delta(\sigma)$, the torque performance and robustness can be evaluated. The maximum value of $\bar{\mu}$ and the minimum values of $\bar{\sigma}$ and $\delta(\sigma)$ for the ST and STPPV of the DFM-MGM are required to obtain the robust optimization designs.

Fig.9 shows the flow charts of the MODO and the developed MORO. In this method, the full factorial design method and the PR technique are adopted to construct the surrogate models of ST and STPPV. Compared with the other non-dominated optimal algorithms, e.g. NSGA-II, the MOPSO algorithm is proven an effective global multi-objective optimization method with fast convergence and well-distributed Pareto fronts [21]. It has also been demonstrated that the MOPSO algorithm is effective to solve the optimization problems of electromagnetic devices [4, 17]. Therefore, the MOPSO algorithm is firstly employed to perform the MODO of the DFM-MGM for maximizing the ST and STPPV without considering any uncertainties. The settings of MOPSO algorithm are listed in Table III. The MOPSO algorithm will then be employed for the MORO based on multiple MCSs to increase the robustness of the optimal results. The number of small segments (N_i) for the interval variable α_p is set as 20. For each small segment of α_p, 10,000 (N=10,000) MCSs are employed for all random variables to obtain the characteristics in statistics. Therefore, the number of hybrid points is equal to 10,000×20=200,000. Then, the robustness of the solutions is evaluated by the multiple MCSs method for each step of the MORO process.

C. Results and discussion

The MOPSO algorithm is employed to obtain the Pareto fronts of MODO without any uncertainties and MORO considering both the random and interval uncertainties of variables. The robustness of MODO results is assessed by the multiple MCSs method, where the same random and interval variables as those of MORO are considered. In order to observe and compare the different effects of $\bar{\sigma}$ and $\delta(\sigma)$ on the robust optimization results, two sets of (λ_1, λ_2) as (0.45, 0.05) and (0.05, 0.45) are respectively selected for optimization. The optimization results of the design parameters by MODO and MORO are given in Table IV. The comparison of Pareto fronts of $\bar{\mu}$ for the MODO and MORO are plotted together in Fig. 10.

This article has been accepted for publication in a future issue of this journal, but has not been fully edited. Content may change prior to final publication. Citation information: DOI 10.1109/TEC.2020.3003402, IEEE Transactions on Energy Conversion

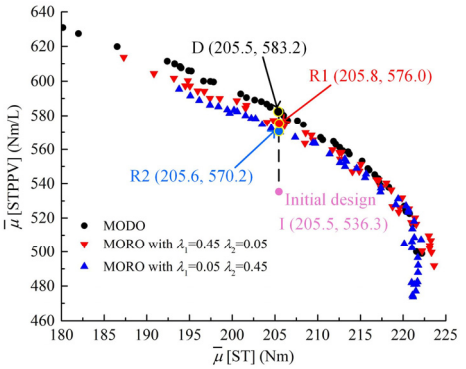

Fig. 10. The Pareto fronts of average means for MODO and MORO.

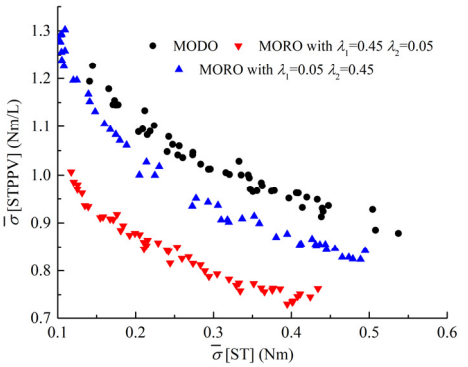

Fig. 11. The Pareto fronts of average standard deviations for MODO and MORO.

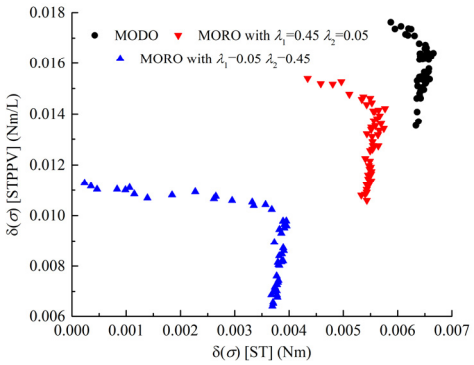

Fig. 12. The Pareto fronts of standard deviation differences for MODO and MORO.

As shown, the Pareto fronts have converged adequately after 1,000 generations. The optimized results show that the MORO with the aforementioned weighting coefficients can achieve an STPPV of 7.5% and 6.3% higher than that of the initial design under the same constraint of ST, respectively. It is also shown that the Pareto fronts of MORO all locate to the left of the MODO solutions, which means the lower average means of ST and STPPV for the MORO results. This is a result that the MORO can reduce the probability of limit violation caused by parameter variation and parametric noise. It is interesting to note that the Pareto fronts obtained by MORO move farther away from those for MODO as the increase of λ_2, indicating the values of $\bar{\mu}$ are worse under more attention to the $\delta(\sigma)$.

Fig. 11 presents the Pareto fronts of $\bar{\sigma}$ for MODO and MORO, respectively. It can also be seen that the average standard deviations obtained by MORO are smaller than those achieved by MODO, indicating that the Pareto fronts become more stable. It is also worth noting that the Pareto fronts obtained by MORO move to the lower left and the ranges become narrower as λ_2 decreases. Conversely, the values of $\delta(\sigma)$ are much lower when the value of λ_2 is higher, as shown in Fig. 12. The aforementioned results also reveal that the optimal designs by MORO are much tighter for the responses of ST and STPPV when the hybrid uncertainties are considered.

TABLE V
ERROR OF OPTIMIZATION METHOD

		MODO	MORO with $\lambda_1=0.45$ $\lambda_2=0.05$	MORO with $\lambda_1=0.05$ $\lambda_2=0.45$
$\bar{\mu}$[ST] (Nm)	Surrogate models	205.45	205.82	205.58
	3D FEM	205.23	205.54	205.37
	Error	0.11%	0.14%	0.10%
$\bar{\mu}$[STPPV] (Nm/L)	Surrogate models	583.19	576.00	570.15
	3D FEM	582.24	575.05	569.06
	Error	0.16%	0.18%	0.20%
$\bar{\sigma}$[ST] (Nm)	Surrogate models	0.35	0.33	0.35
	3D FEM	0.35	0.33	0.35
	Error	0.25%	0.44%	0.49%
$\bar{\sigma}$[STPPV] (Nm/L)	Surrogate models	0.97	0.79	0.88
	3D FEM	0.97	0.79	0.88
	Error	0.34%	0.47%	0.15%
$\delta(\sigma$[ST]) (Nm)	Surrogate models	$6.43*10^{-3}$	$5.74*10^{-3}$	$3.81*10^{-3}$
	3D FEM	$6.42*10^{-3}$	$5.72*10^{-3}$	$3.80*10^{-3}$
	Error	0.16%	0.35%	0.29%
$\delta(\sigma$[STPPV]) (Nm/L)	Surrogate models	$1.54*10^{-2}$	$1.12*10^{-2}$	$0.75*10^{-2}$
	3D FEM	$1.53*10^{-2}$	$1.12*10^{-2}$	$0.75*10^{-2}$
	Error	0.48%	0.46%	0.45%

TABLE VI
COMPARISON OF MODO AND MORO

	MODO	MORO with $\lambda_1=0.45$ $\lambda_2=0.05$	MORO with $\lambda_1=0.05$ $\lambda_2=0.45$
$\bar{\mu}$[ST]	207.63 Nm	209.27 Nm	213.18 Nm
$\bar{\mu}$[STPPV]	576.98 Nm/L	568.27 Nm/L	554.33 Nm/L
$\bar{\sigma}$[ST]	0.32 Nm	0.29 Nm	0.31 Nm
$\bar{\sigma}$[STPPV]	1.01 Nm/L	0.79 Nm/L	0.91 Nm/L
$\delta(\sigma$[ST])	$6.50*10^{-3}$ Nm	$5.50*10^{-3}$ Nm	$3.82*10^{-3}$ Nm
$\delta(\sigma$[STPPV])	$1.57*10^{-2}$ Nm/L	$1.26*10^{-2}$ Nm/L	$0.84*10^{-2}$ Nm/L

Table V compares the optimal results of MODO and MORO. As shown, these errors of optimization results based on surrogate models are 0.5% less than the 3D FEM results, which demonstrates the effectiveness of MORO method with multiple MCSs. It can also be seen that the STPPV achieved by MORO is slightly lower than those by MODO under the same constraint of ST. The values of $\bar{\sigma}$ and $\delta(\sigma)$ are much lower than those obtained by MODO. The above results clearly show a compromise must be made between the robustness and the utilization of PMs at the same value of ST.

The probability density function (PDF) can describe a variable by defining the probability of its occurrence in statistics. In order to directly reveal the effects of both the random and interval uncertainties of design parameters on the robustness of ST and STPPV achieved by MODO and MORO, respectively, the families of PDF distributions are presented in Fig. 13. The distribution range of the MORO with λ_1=0.45 and λ_2=0.05 is slightly narrower than that of the MODO, as shown in Figs. 13 (a) and (c). Compared with the bound of distribution

This article has been accepted for publication in a future issue of this journal, but has not been fully edited. Content may change prior to final publication. Citation information: DOI 10.1109/TEC.2020.3003402, IEEE Transactions on Energy Conversion

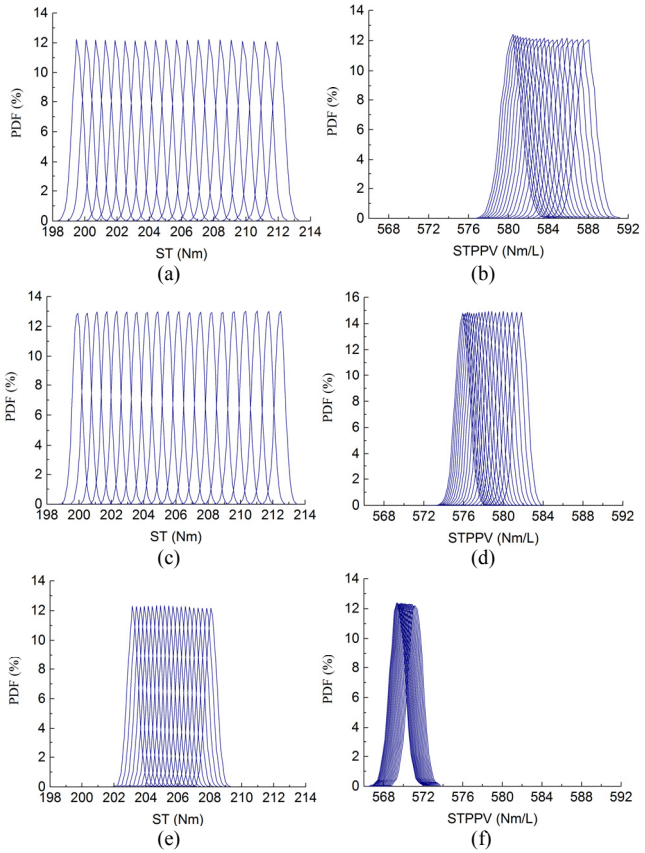

Fig. 13. The distributions graphs. (a) and (b) ST and STPPV from MODO, (c) and (d) ST and STPPV from MORO with λ_1=0.45, λ_2=0.05, (e) and (f) ST and STPPV from MORO with λ_1=0.05, λ_2=0.45.

shown in Fig. 13 (a), the bound for MORO with λ_2=0.45 is much closer to that shown in Fig. 13 (e). The variation of distributions for the STPPV shown in Figs. 13 (b), (d) and (f) is similar to that for the ST. It can also be seen that the range and bound of the distributions for the solutions obtained by MORO may shrink with smaller values of $\bar{\sigma}$ and $\delta(\sigma)$. Hence, it is proven that the robustness of optimization results obtained by MORO can be significantly improved. The range and bound of the distributions are evidently much narrower with more emphasis on $\delta(\sigma)$, indicating that λ_2 may have bigger impact on the robustness of optimization results than λ_1.

While the Pareto fronts can be obtained by MODO and MORO, it is difficult to choose an overall optimal design result from the Pareto fronts. Since each point on the Pareto fronts represents one Pareto optimal solution, two objective functions can be conflicting. In this paper, three overall optimization points from the Pareto fronts shown in Fig. 10 are picked up by adopting the normalized minimum distance selection method presented in [22]. The results are compared in Table VI. As shown, the average standard deviations and standard deviation differences of the ST and STPPV obtained by MORO are lower than those by MODO, meaning that the robustness of optimal results can be improved by MORO. A bigger λ_2 may yield lower standard deviation differences and higher average standard deviations of the optimization results obtained by MORO. Therefore, a trade-off must be made between $\bar{\sigma}$ and $\delta(\sigma)$ of the ST and STPPV in the process of MORO.

V. Conclusion

The MORO approach considering both the random and interval uncertainties proposed in this paper can improve the torque performance and robustness of the DFM-MGM design simultaneously. The optimized results show that the STPPV of DFM-MGM achieved by MORO is 6.3% higher than that of the initial design with the same ST. Compared with the MODO results, the optimized counterparts obtained by the MORO method can remarkably reduce the values of $\bar{\sigma}$ and $\delta(\sigma)$ for the optimization results induced by the hybrid uncertainties of variables. Furthermore, the weighting coefficient λ_2 is found to have bigger effects on both the range and bound of the distributions for the Pareto solutions than λ_1, indicating that the robust design with the interval uncertainty has a higher requirement for robustness. It is proven that the proposed MORO approach is effective to improve the robustness and torque performance of DFM-MGM by considering the hybrid uncertainties of design parameters. Consequently, the proposed method may potentially provide an alternative decision maker of robustness problems and new insights into the MORO for DFM-MGMs. In addition, the MORO design methodology employed in this paper can be applicable to other types of electrical machines to achieve optimal designs robust to the hybrid uncertainties.

Acknowledgment

This work was supported in part by the National Natural Science Foundation of China under Grant 51877074.

References

[1] J. M. Crider and S. D. Sudhoff, "An inner rotor flux-modulated permanent magnet synchronous machine for low-speed high-torque applications," *IEEE Trans. Energy Convers.,* vol. 30, no. 3, pp. 1247–1254, Sep. 2015.

[2] X. Zhang, X. Liu, Y. Zhao, and Z. Chen, "A novel magnetic-geared machine with dual flux modulators," in *Proc. IEEE Annu. Conf. Ind. Electron. Soc.*, Oct. 2018, pp. 349–354.

[3] Q. Wang, S. Niu, and L. Yang, "Design optimization and comparative study of novel dual-PM excited machines," *IEEE Trans. Ind. Electron.,* vol. 64, no. 12, pp. 9924–9933, Dec. 2017.

[4] A. Cavagnino, G. Bramerdorfer, and J. A. Tapia, "Optimization of electric machine designs—Part I," *IEEE Trans. Ind. Electron.,* vol. 64, no. 12, pp. 9716–9720, Dec. 2017.

[5] G. Lei, C. Liu, J. Zhu, and Y. Guo, "Techniques for multilevel design optimization of permanent magnet motors," *IEEE Trans. Energy Convers.,* vol. 30, no. 4, pp. 1574–1584, Dec. 2015.

[6] Y. C. Wang, S. Niu, and W. Fu, "Sensitivity analysis and optimal design of a dual mechanical port bidirectional flux-modulated machine," *IEEE Trans. Ind. Electron.,* vol. 65, no. 1, pp. 211–220, Jan. 2018.

[7] P. Asef, R. Bargallo, M. R. Barzegaran, A. C. Lapthorn, and D. Mewes, "Multi-objective design optimization using dual-level response surface methodology and booth's algorithm for permanent magnet synchronous generators," *IEEE Trans. Energy Convers.*, vol. 33, no. 2, pp. 652–659, Jun. 2018.

[8] G. Lei, T. Wang, J. Zhu, Y. Guo, and S. Wang, "System-level design optimization method for electrical drive systems-robust approach," *IEEE Trans. Ind. Electron.,* vol. 62, no. 8, pp. 4702–4713, Aug. 2015.

[9] G. Bramerdorfer and A. C. Zavoianu, "Surrogate-based multi-objective optimization of electrical machine designs facilitating tolerance analysis," *IEEE Trans. Magn.*, vol. 53, no. 8, Aug. 2017, Art. no. 8107611.

[10] M. Z. Islam, A. Arafat, S. S. R. Bonthu, and, S. Choi, "Design of a robust five-phase ferrite-assisted synchronous reluctance motor with low demagnetization and mechanical deformation," *IEEE Trans. Energy Convers.,* vol. 34, no. 2, pp. 722–730, Jun. 2019.

[11] B. Ma, G. Lei, J. Zhu, Y. Guo, and C. Liu, "Application-oriented robust design optimization method for batch production of permanent-magnet

motors," *IEEE Trans. Ind. Electron.,* vol. 65, no. 2, pp. 1728–1739, Feb. 2018.
[12] S. Yang, J. Yang, Y. Bai, and G. Ni, "A new methodology for robust optimizations of optimal design problems under interval uncertainty," *IEEE Trans. Magn.,* vol. 52, no. 3, Mar. 2016, Art. no. 7001104.
[13] B. Ma, J. Zheng, G. Lei, J. G. Zhu, Y. G. Guo, and J. L. Wu, "A robust design optimization method for electromagnetic devices with interval uncertainties," *IEEE Trans. Magn.,* vol. 54, no. 11, Nov. 2018, Art. no. 8107804.
[14] C. Qiu, X. Peng, Z. Liu, and J. Tan, "Sensitivity analysis of random and interval uncertain variables based on polynomial chaos expansion method," *IEEE Access*, vol. 7, pp. 73046–73056, 2019.
[15] J. Cheng, W. Lu, W. Hu, Z. Liu, Y. Zhang, and J. Tan, "Hybrid reliability-based design optimization of complex structures with random and interval uncertainties based on ASS-HRA," *IEEE Access*, vol. 7, pp. 87097–87109, 2019.
[16] X. Zhang, X. Liu, and Z. Chen, "A novel dual-flux-modulator coaxial magnetic gear for high torque capability," *IEEE Trans. Energy Convers.,* vol. 33, no. 2, pp. 682–691, Jun. 2018.
[17] G. Bramerdorfer, J. A. Tapia, J. J. Pyrhönen, and A. Cavagnino, "Modern electrical machine design optimization: Techniques, trends, and best practices," *IEEE Trans. Ind. Electron*., vol. 65, no. 10, pp. 7672–7684, Oct. 2018.
[18] K. Li, S. Modaresahmadi, W. B. Williams, J. Z. Bird, J. D. Wright and D. Barnett, "Electromagnetic analysis and experimental testing of a flux focusing wind turbine magnetic gearbox," *IEEE Trans. Energy Convers.,* vol. 34, no. 3, pp. 1512–1521, Sept. 2019.
[19] S. Gerber and R. Wang, "Design and evaluation of a magnetically geared PM machine," *IEEE Trans. Magn.*, vol. 51, no. 8, Aug. 2015, Art no. 8107010.
[20] S. Xiao, Y. Li, M. Rotaru, and J. K. Sykulski, "Six sigma quality approach to robust optimization," *IEEE Trans. Magn.*, vol. 51, no. 3, Mar. 2015, Art. no. 7201304.
[21] C. Coello, G. Pulido, and M. Lechuga, "Handling multiple objectives with particle swarm optimization," *IEEE Trans. Evol. Comput.,* vol. 8, no. 3, pp. 256–279, Jun. 2004.
[22] D. Zhang, Z. Ren, and C.-S. Koh, "Optimal design of powder-aligning and magnetizing fixtures for an anisotropic-bonded NdFeB permanent magnet," *IEEE Trans. Magn.,* vol. 50, no. 2, Feb. 2014, Art. no. 7017204.

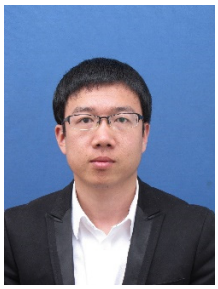

Xiao Liu (M'14–SM'19) was born in Harbin, China, in 1981. He received the B.Eng. and Ph.D. degrees in electrical engineering from Zhejiang University, Hangzhou, China, in 2003 and 2008, respectively.

From 2008 to 2011, he was a Postdoctoral Researcher with Zhejiang University, Hangzhou, China. He was a Postdoctoral Researcher and Assistant Professor with Aalborg University, Denmark during 2012-2015. Since 2016, he has been an Associate Professor of electrical engineering with Hunan University.

His main research interests include design and control of the renewable energy power generator, direct-drive electrical machines, permanent magnet linear machines, magnetic gear and magnetic geared machines. He has published more than 30 technical papers.

Yunyun Zhao received the M.Sc. degree in mechanical engineering from Hunan University, Changsha, China, in 2017. He is currently working toward the Ph.D. degree in electrical engineering, Hunan University, Changsha, China.

His major research interests include the analysis and design of magnetic gears and magnetic gear machines for high-torque application.

Jianguo Zhu (S'93–M'96–SM'03) received the B.E. degree in 1982 from Jiangsu Institute of Technology, Jiangsu, China, the M.E. degree in 1987 from Shanghai University of Technology, Shanghai, China, and the Ph.D. degree in 1995 from the University of Technology Sydney (UTS), Sydney, Australia, all in electrical engineering.

He was appointed a lecturer at UTS in 1994 and promoted to full professor in 2004 and Distinguished Professor of Electrical Engineering in 2017. At UTS, he has held various leadership positions, including the Head of School for School of Electrical, Mechanical and Mechatronic Systems and Director for Centre of Electrical Machines and Power Electronics. In 2018, he joined the University of Sydney, Australia, as a full professor and Head of School for School of Electrical and Information Engineering. His research interests include computational electromagnetics, measurement and modelling of magnetic properties of materials, electrical machines and drives, power electronics, renewable energy systems and smart micro grids.

Zhe Chen (M'95–SM'98) received the B.Eng. and M.Sc. degrees from Northeast China Institute of Electric Power Engineering, Jilin, China, and the Ph.D. degree from the University of Durham, Durham, U.K.

He is a Full Professor with the Department of Energy Technology, Aalborg University, Denmark. He is the Leader of Wind Power System Research Program at the Department of Energy Technology, Aalborg University, Aalborg, Denmark and the Danish Principle Investigator for Wind Energy of Sino-Danish Centre for Education and Research.

His research areas cover power systems, power electronics and electric machines with current main interests in wind energy and modern power systems. He has led many research projects and has more than 500 publications in his technical field. He is an Associate Editor of the IEEE TRANSACTIONS ON POWER ELECTRONICS, a member of editor boards for a number of international journals, a Fellow of the Institution of Engineering and Technology (London, U.K.), and a Chartered Engineer in the U.K.

Shoudao Huang (M'13–SM'14) was born in Hunan, China, in 1962. He received the B.S. and Ph.D. degrees in electrical engineering from Hunan University, Changsha, China, in 1981 and 2005, respectively.

Since 2006, he has been a Professor in electrical engineering at the College of Electrical and Information Engineering, Hunan University. His interests include distributed power generation and motor driver and control.